

# Evaluation of a high-resolution historical simulation over China: climatology and extremes

Entao Yu · Jianqi Sun · Huopo Chen · Weiling Xiang

Received: 24 July 2014 / Accepted: 13 December 2014 / Published online: 25 December 2014  
© Springer-Verlag Berlin Heidelberg 2014

**Abstract** China faces an increasing challenge in water resources in the coming decades; thus high-confidence climate projection is of particular importance for the country's future. In this paper, we evaluate the performance of a long high-resolution continuous simulation over China based on multiple observations and the corresponding historical simulation. The simulation is completed using the Weather Research and Forecasting (WRF) model driven by the Model for Interdisciplinary Research on Climate version 5 (MIROC5) in the context of the Coupled Model Intercomparison Project Phase 5. The results show that both MIROC5 and WRF can capture the distribution and variability of temperature over China, whereas WRF shows improvements, particularly for simulation of regional features. Compared with MIROC5, WRF can reproduce the spatial distribution, annual cycle, probability distribution, and seasonal evolution of the precipitation over mainland China and the sub-regions with better performance. The trend is of fundamental

importance in the future projection estimations, and WRF shows better skill in simulating the annual mean precipitation trend. However, there is overestimation of precipitation in Southeast China while negative one in the middle latitude of China in WRF simulation, which can be traced back to model bias in atmospheric circulation and water vapor transportation in these regions. Several extreme climate indices are selected to further assess the model's performance in simulating climate extremes, WRF can well reproduce the main features with better model skill compared with MIROC5. The better performance of WRF indicates the necessity of the dynamical downscaling technique and the robustness of regional climate simulation in future regional climate projection over China.

**Keywords** Model evaluation · Regional climate models · China · Climatology and extremes

---

E. Yu (✉) · J. Sun · H. Chen  
Nansen-Zhu International Research Centre, Institute  
of Atmospheric Physics, Chinese Academy of Sciences,  
Beijing 100029, China  
e-mail: yetsyu@mail.iap.ac.cn

E. Yu · J. Sun · H. Chen  
Climate Change Research Center, Chinese Academy of Sciences,  
Beijing 100029, China

H. Chen  
Collaborative Innovation Center on Forecast and Evaluation  
of Meteorological Disasters, Nanjing University of Information  
Science & Technology, Nanjing 210044, China

W. Xiang  
State Key Laboratory of Atmospheric Boundary Layer Physics  
and Atmospheric Chemistry, Institute of Atmospheric Physics,  
Chinese Academy of Sciences, Beijing 100029, China

## 1 Introduction

Although China has the largest population, its agriculture land is limited. Due to the vulnerability of water resources in this region, climate change, particularly precipitation variation, is of essential importance (Vörösmarty et al. 2000). Anomalies in precipitation play an important role in this agricultural and rapidly developing country. The increasing demand of water resources due to the growing population, rapid economic development, and extensive urbanization indicates that China faces severe challenges in water resources at present and these challenges could be more serious in the future (Piao et al. 2010). Furthermore, extreme climates such as intense snowfall, heat waves, drought, flooding, and freezing rain occur more frequently in the warming world, which brings large economic losses and economic

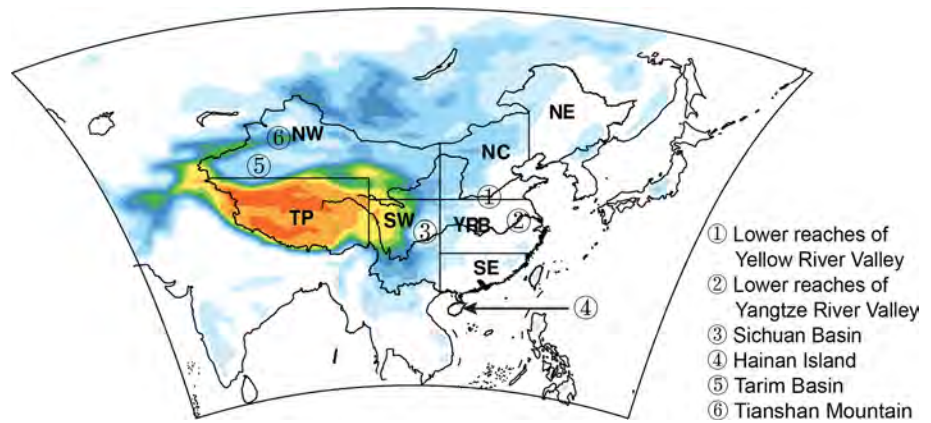
threats to China (Sun et al. 2010, 2011; Chen et al. 2013; Sun 2014; Ding et al. 2008). Due to the severe freezing disaster in South China in 2008 (Chen et al. 2011), for example, more than 2 million homes or roofs collapsed in 20 provinces, 12 million hectares of crops were damaged, and the economic losses were estimated at 151 billion Yuan (Hu et al. 2010). In addition, the severe drought event of 2009–2010 in south-western China caused drinking water shortages for approximately 21 million people, and the economic losses reached nearly 180 billion Yuan (Yang et al. 2012). Recent observations indicate significant changes in precipitation over China. For instance, Sun and Ao (2013) suggested that winter precipitation and extreme precipitation are increasing in the warming environment in China. Wang and He (2013) found that the snowfall in Northeast China increased approximately 20 % during 1986–2010 over Northeast China than that in 1951–1985. The authors suggested it is associated to the East Asian winter monsoon; other studies have stressed the influence of Arctic sea ice (Liu et al. 2012a). Zhu et al. (2011) found that precipitation over East China increased in the Huang-Huai River region and decreased in the Yangtze River region during 2000–2008 in comparison to 1979–1999, which may be related to the decadal change of the Pacific decadal oscillation (PDO). The previous multidecadal variation in precipitation over China is associated with the East Asia monsoon system, which is a hybrid of tropical and subtropical monsoons (Yang et al. 2014; Ding and Chan 2005), and the variation can also be related to the North Atlantic Oscillation (Sun and Wang 2012), El Niño Southern Oscillation (ENSO; Fu et al. 2013; He and Wang 2013), anthropogenic aerosols (Wang et al. 2013), the Indian Ocean, the Tibetan Plateau, and internal variability (Zhou et al. 2009). Thus, high-confident climate projection is quite important for China's future development.

Coupled global climate models forced by projected greenhouse gas and aerosol emissions in the Coupled Model Inter-comparison Project Phase 5 (CMIP5) are the primary tools for estimating trends and variability of future climate and extremes, and the results are used to evaluate future climate change under various representative concentration pathways (RCP) scenarios. Based on the results of CMIP5, several studies have evaluated the changes in precipitation, flood/drought, and extreme climate events over China under different RCP scenarios (e.g., Xu and Xu 2012; Chen 2013; Chen et al. 2013). These results enabled a more comprehensive understanding of the future climate under different scenarios from the latest generation of state-of-the-art global climate models (GCMs). However, the horizontal resolution of CMIP5 models spans from 100 to 300 km (Taylor et al. 2011), which is coarse in resolving mesoscale or regional scale climate features. The World Climate Research Program (WCRP) recently initiated the coordinated regional climate downscaling experiment (CORDEX, Giorgi et al. 2009),

which provides high-resolution regional climate change projections on land areas worldwide by using regional climate models (RCMs). Endris et al. (2013) evaluated the performances of RCMs from CORDEX in simulating rainfall over eastern Africa, it is found that most RCMs reasonably simulate the main features of the rainfall climatology, at the same time the analysis shows significant biases in individual models depending on sub-region and season; Vautard et al. (2013) evaluated the simulation of European heat waves, and found most models exhibited an overestimation of summertime temperature extremes in Mediterranean regions and an underestimation over Scandinavia even after bias removal, but a higher resolution reduced this deficiency; In North America, very high-resolution (4–12 km) dynamical downscaling simulations were conducted, and the RCMs shows quite good performances (Caldwell et al. 2009; Gao et al. 2012a; Pan et al. 2011; Martynov et al. 2013). There were also dynamical downscaling simulations over East Asia, and the studies indicated that RCMs can reproduce the spatial distribution of mean climate and extreme climate events better (Gao et al. 2008, 2011, 2012b; Yu et al. 2010; Wang et al. 2011; Lee et al. 2014).

Most of the previous dynamical downscaling simulations were based on CMIP3 outputs, which had coarser resolution and older emission scenarios, and they mainly focused on the temperature and precipitation climatology, therefore, the changes in extreme climate projected by high resolution regional climate models with newly developed CMIP5 outputs is especially meaningful over China considering its peculiarities and vulnerability. In this paper, historical (1946–2005) and future projection (2006–2100) simulations over China have been conducted using WRF model driven by the Model for Interdisciplinary Research on Climate version 5 (MIROC5) in the context of CMIP5, it contributes to the existing information on regional climate change over China by supplying with high resolution (30 km) simulations with newly-developed RCP of CMIP5, the simulation have been completed with WRF model which was not included in the aforementioned studies over China. In addition, this paper provides the evaluation of the performance of WRF model in simulating the climate extremes represented by indices as compared to GCM and observations, the indices are calculated with a consistent methodology of Expert Team on Climate Change Detection and Indices (ETCCDI) across all the datasets, which has not been included in previous research. The primary objective of this paper is to identify the models' performances over China by comparing the historical run with multiple observation data, mainly focusing on climatology and extremes. The remainder of this paper is as follows: Sect. 2 describes the models and the observation data and Sect. 3 evaluates the model performance with the historical run. Finally, Sect. 4 concludes the study with a discussion.

**Fig. 1** Computation domain of WRF (within the *outer black line*) and seven sub-regions [Northeast China (NE), North China (NC), the Yangtze River Basin (YRB), Southeast China (SE), Southwest China (SW), Northwest China (NW), and the Tibetan Plateau (TP)], *shading* indicates the topography, and *warm colors* stand for higher elevation, six locations in China are labelled with *number*



## 2 Model, experiment design, and observation data

### 2.1 Model description

The global coupled climate model used in this study is the MIROC5, which is developed on the basis of MIROC3.2, the atmosphere model is the Center for Climate System Research, University of Tokyo (CCSR)/National Institute for Environmental Studies (NIES)/Frontier Research Center for Global Change (FRCGC) AGCM, which is based on a global spectral dynamical core and includes a standard physics package. The ocean model is the CCSR Ocean Component Model (COCO), which includes a sea ice model. MIROC5 also couples a land model that includes a river module. Further details of MIROC5 have been reported by Watanabe et al. (2010).

The regional climate model used in this study is the WRF version 3.4, which is a mesoscale numerical model consisting of a model solver of fully compressible Eulerian and nonhydrostatic equations with a run-time hydrostatic option (Skamarock et al. 2008). The model uses a terrain-following coordinate with the top of the model being a constant pressure surface. The horizontal grid is the Arakawa-C grid, and the time integration scheme in the model uses the third-order Runge–Kutta scheme. This model has been widely used in regional climate studies over China, and the studies indicated that the model can reproduce the main features of climate in this region well (Ge et al. 2013; Yang et al. 2014; Yu 2012).

### 2.2 Experimental design

The main model configurations of WRF in the continuous integration are as follows. The microphysics are parameterized by the Single-Moment 6-class Microphysics (WSM6) scheme including ice, graupel, and their associated processes (Hong and Lim 2006); the radiation transfer schemes for longwave and shortwave are modeled by the National Center for Atmospheric Research (NCAR) Community

Atmosphere Model (CAM 3.0), which can handle several trace gases and interacts with resolved clouds and cloud fractions (Collins et al. 2004); the surface layer is depicted by the Fifth-Generation Penn State/NCAR Mesoscale Model (MM5) Monin–Obukhov scheme (Skamarock et al. 2008); the land surface process is modeled by the Noah land surface model with multiparameterization options (Noah–MP; Niu et al. 2011; Yang et al. 2011); the cumulus convective precipitation is parameterized by the Kain–Fritsch scheme (Kain 2004), and the planetary boundary layer is depicted by the Yonsei University scheme (Hong et al. 2006).

The WRF domain covers mainland China and the nearby regions with the spatial resolution of 30 km under the Lambert conformal map projection (Fig. 1). Validations that are more detailed will be presented for seven sub-regions with various climate features, including Northeast China (NE), North China (NC), the Yangtze River Basin (YRB), Southeast China (SE), Southwest China (SW), the Tibetan Plateau (TP) and Northwest China (NW). The initial and boundary conditions for WRF were obtained from the MIROC5 historical and RCP60 experiments for 1946–2100 in CMIP5 at a time frequency of 6 h. The code of WRF model was adapted to include the mixing ratio of greenhouse gas (GHG) for the new RCP scenario used in CMIP5. The results of 1986–2005 in the historical run were chosen as the present-day climatology, which is consistent with the definition of the Fifth Assessment Report of the United Nations Intergovernmental Panel on Climate Change (IPCC AR5; IPCC 2013).

### 2.3 Observation data and statistical methods

Due to uncertainties in the data sources and processing algorithm, the observation products also have potential uncertainties; thus, they can provide only possibilities for the observational truth (Xu and Powell 2012). In this paper, we use multiple observation products to evaluate the model's skill in simulating the surface air temperature,

precipitation and extreme climate indices for 1986–2005 in the historical run, namely the CN05 daily mean temperature, daily maximum temperature, daily minimum temperature and daily precipitation data from China Meteorological Administration (CMA; Wu and Gao 2013), the University of East Anglia Climatic Research Unit (CRU) TS3 monthly temperature and precipitation data (Mitchell and Jones 2005), the Asian Precipitation–Highly Resolved Observational Data Integration Towards Evaluation of Water Resources (APHRODITE, hereafter APHRO for short) daily temperature and precipitation data (Yatagai et al. 2012), and the Global Precipitation Climatology Project (GPCP) monthly precipitation data (Huffman et al. 2009). The CN05 product contains daily mean temperature, maximum temperature, minimum temperature, and precipitation at a horizontal resolution of  $0.25^\circ \times 0.25^\circ$ , it is developed on the basis of more than 2,400 meteorological stations in mainland China. The CRU data contains global monthly temperature and precipitation at the resolution of  $0.5^\circ \times 0.5^\circ$ . The APHRO product contains daily temperature and precipitation over Asia, and its resolution is  $0.25^\circ \times 0.25^\circ$ . The GPCP includes satellite–gauge combination data starting from 1979, which contains only precipitation with a resolution of  $2.5^\circ \times 2.5^\circ$ . There are also other observation products over the regions of interest, such as the Tropical Rainfall Measuring Mission (TRMM; Huffman et al. 2007) and the Climate Prediction Center morphing method (CMORPH; Joyce et al. 2004), however, these products do not cover the entire 1986–2005 period. In addition to the temperature and precipitation, we also use the wind from Climate Forecast System Reanalysis (CFSR) data, which have a resolution of  $0.5^\circ \times 0.5^\circ$  (Saha et al. 2010). The pattern correlation (PCOR), standard deviation (SD), model anomaly bias (BIAS) and root mean square difference (RMSD) are used to assess model's performance.

### 3 Results

#### 3.1 Temperature

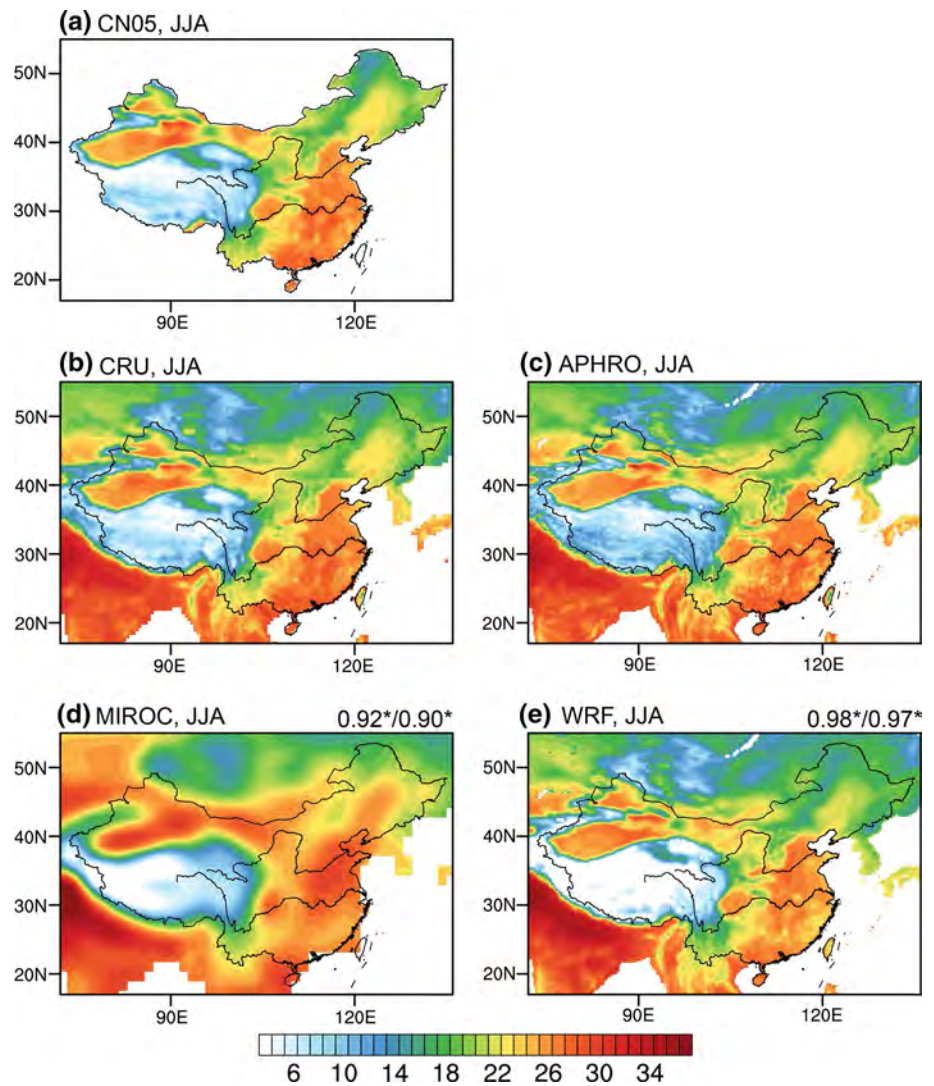
Figure 2 illustrates the seasonal averaged temperature during 1986–2005 for June–July–August (JJA) obtained from observations and model simulations. The CN05, CRU, and APHRO agree well with each other, and the observations indicate that the summer mean temperature decreases from south to north over China. The hot center appears in Southeast China, where the summer mean temperature ranges between 24 and 27 °C with the maximum temperature exceeding 27 °C in Hainan Island, the coastal regions of South China, and the middle reaches of the Yangtze River Valley. The cold center is located in the Tibetan Plateau,

with a summer mean temperature lower than 3 °C due to its topography. MIROC5 captures the large-scale distribution of summer mean temperature while fails to reproduce the regional features. For instance, the simulated hot center extends to the lower reaches of Yellow River Valley, which is approximately  $5^\circ\text{N}$  of the observation. In addition, MIROC5 also misses many details in regional scale, such as the low temperature in Tianshan Mountain in Northwest China. However, WRF gains many improvements compared with MIROC5, and the simulation agrees with the observation better, particularly for the regional features in Southeast China, the Yangtze River Valley and Northwest China. For instance, WRF captures the temperature distribution over Sichuan Basin and Tarim Basin with better agreement with the observation. The correlation coefficients between observation and simulations are about 0.9 for MIROC5 and 0.97 for WRF, which indicates that WRF has significantly better performance for the temperature simulations.

To assess the model's ability in simulating the temperature variability over China, we calculated the standard deviation of temperature for JJA during 1986–2005 (Fig. 3). Although there are differences among the observations, all of the observational products indicate that the variability of temperature increases from south to north. MIROC5 and WRF reproduce the spatial pattern of temperature variability well, including the large variability in high latitude and the small one in lower latitude over China. WRF simulation shows improvements mainly in regional scale, including the regions of Southwest China and North China. However, both models indicate large variability over the Tibetan Plateau, which disagrees with the observation, these biases indicate challenges for temperature simulation over high topography regions, even for the high-resolution RCM simulations.

Table 1 shows the annual and seasonal mean PCOR, anomaly BIAS and RMSD over the entire China and the sub-regions between CN05 observation and the corresponding model simulation. When we calculate the anomaly BIAS and RMSD, we first subtract the model's climatology (1976–2005) to remove the systematic model bias. The PCORs of MIROC5 for China and the sub-regions are approximately 0.9, indicating good performance in reproducing the spatial distribution of temperature. Higher PCORs of MIROC5 appear in the regions of Northeast China, North China, and Northwest China, whereas lower values appear in the Yangtze River Basin, the Tibetan Plateau, and Northwest China. WRF shows significant improvements with higher PCORs over all regions. The most obvious improvements appears in the Yangtze River Basin, the Tibetan Plateau, and Northwest China, which can be traced back to the weakness of MIROC5 in these regions. For anomaly BIAS and RMSD aspects, WRF also

**Fig. 2** Summer mean temperature (units: °C) during 1986–2005 from the **a** CN05, **b** CRU, **c** APHRO, **d** MIROC5 and **e** WRF for June–July–August (JJA), the correlation coefficients between the simulations and the observation (CN05 and APHRO products are selected as the observation due to their high resolution) was labelled on the *top-right* of the figure, and *asterisks* indicate the significance level are higher than 90 %



shows improvements, which mainly appears in summer season. WRF's performance is worse in the cold seasons, which was also reported by Liu et al. (2012b). The authors suggested that the decline may be related to the model's deficiency in representing the snow feedback processes; however, further investigation is required to determine the mechanisms for such deficiency.

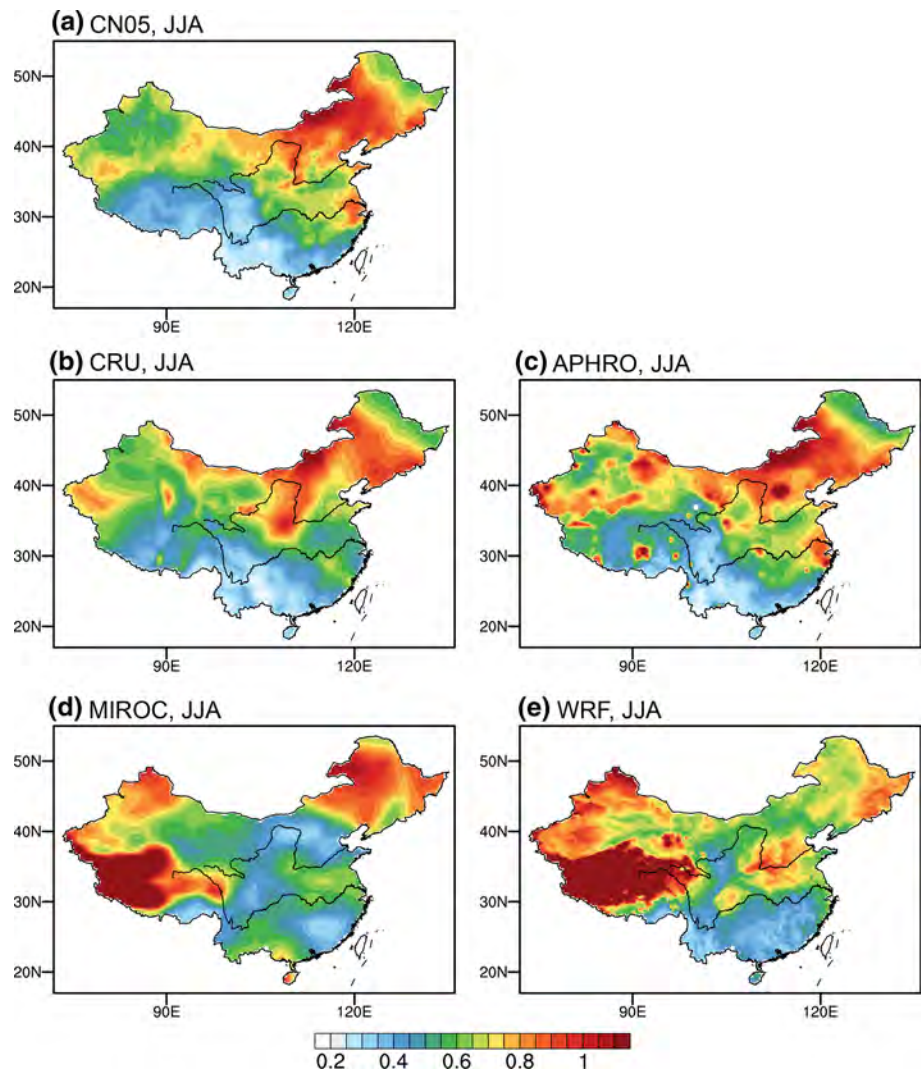
## 3.2 Precipitation

### 3.2.1 Model evaluation

Figure 4 compares the summer mean precipitation from observations and model simulations. The observations indicate precipitation decreases from southeast to northwest over China. The maximum precipitation appears in Southeast China with values exceeding 800 mm, whereas the minimum precipitation is located in Northwest China with values less than 100 mm. However, some differences exist

among the observations, particularly over Northwest China and the Tibetan Plateau, where meteorological stations are quite scarce. MIROC5 and WRF well reproduce the spatial pattern of summer rainfall, although obvious overestimations are observed in Southeast China. The correlation coefficient between observation (CN05/APHRO) for WRF is 0.86/0.85, while for MIROC5 is 0.85/0.84. The improvement is due to the fact that WRF can capture more detailed rainfall features in regional scale due to its finer resolution. For example, the precipitation pattern, as well as the precipitation amount over Northwest China simulated by WRF agrees with CN05 and APHRO better. The false precipitation center over Sichuan Basin is obvious in MIROC5 simulation, whereas WRF can improve it. In the southeastern edge of the Tibetan Plateau, MIROC5 simulates much stronger precipitation than the observation, which may be related to the topographic effect. The Himalayas are much lower in the GCMs due to the coarse resolution, so the precipitation can penetrate into the Plateau (Gao et al. 2008).

**Fig. 3** Same as Fig. 2, but for standard deviation of temperature, unit: °C



Due to the finer resolution, WRF can improve the situation with much better agreement with the observation.

Figure 5 shows the annual cycle of precipitation from observations and simulations. Good agreements are observed among the observations, which indicates the seasonal features of more precipitation in summer and less in winter over China. MIROC5 and WRF capture the main features of seasonal variation, although overestimation is obvious throughout the year, especially in summer. Both models show the largest wet bias in Southeast China in summer, as shown in Fig. 4e, f. WRF shows better performance and less bias, particularly in the regions of North China, Northwest China, Southwest China, and the Tibetan Plateau. In the regions of the Tibetan Plateau and Northwest China, annual precipitation variation and amount simulated by WRF are comparable with the observation.

We also compare the seasonal evolution of the rainfall belt in eastern China, which is closely associated with the East Asia summer monsoon and the drought/flooding in

eastern China. Figure 6 illustrates the latitude–time cross-section of the precipitation averaged over the regions of 110°–125°E from the observations and model simulations. Similarities are observed in the observations, which indicates that the rainfall belt shifts northward in April and reaches the Yangtze River Valley (approximately 30°N) in May before reaching North China in June and July and retreating in August. MIROC5 and WRF reproduce the rainfall evolution reasonably well; however, the overestimation of precipitation is obvious in South China. The intensity of the simulated rainfall in South China is much stronger, and the duration is longer than that of the observation. MIROC5 simulates stronger rainfall between 35°N and 40°N in June and July with values exceeding 7 mm/day, whereas WRF improves the simulation and shows less model bias.

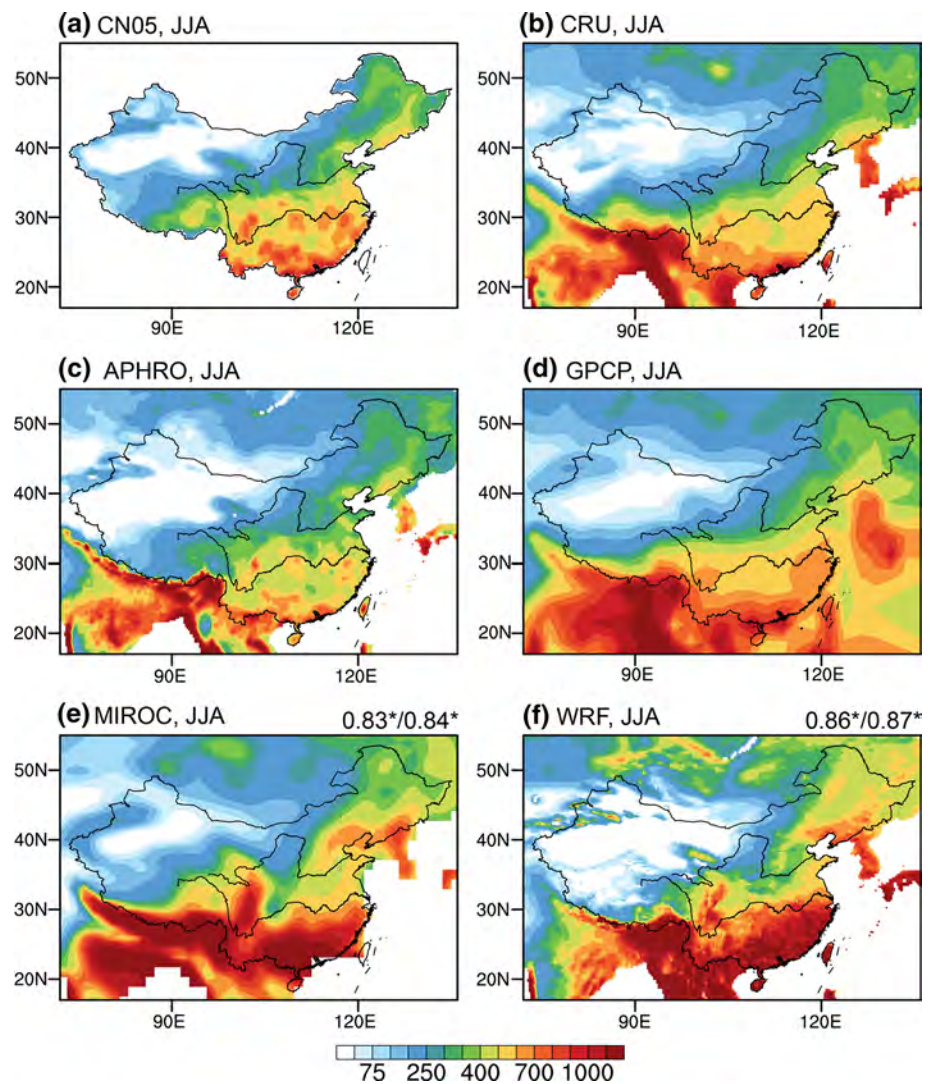
Figure 7 compares the probability distribution of precipitation from observations and simulations. For the temporal averaged precipitation (Fig. 7a), large differences are

**Table 1** Spatial pattern correlation coefficient (PCOR), model bias (BIAS) and root mean square difference (RMSD) over China and sub-regions for annual and seasonal mean temperature between CN05 and MIROC5/WRF simulation, the model climatology (1976–2005) was removed before the calculation of anomaly BIAS and RMSD, ANN stands for annual, MAM for March–April–May, SON for September–October–November, DJF for December–January–February

	PCOR		Anomaly BIAS		Anomaly RMSD	
	MIROC5	WRF	MIROC5	WRF	MIROC5	WRF
China						
ANN	0.94	0.98	−0.12	−0.08	0.7	0.7
MAM	0.93	0.98	−0.29	−0.28	1.47	1.44
JJA	0.92	0.98	0.06	0.0007	0.85	0.88
SON	0.94	0.98	−0.01	0.03	0.92	1.0
DJF	0.93	0.95	−0.17	−0.13	1.37	1.64
Northeast China (NE)						
ANN	0.96	0.96	−0.24	−0.26	0.61	0.61
MAM	0.93	0.95	−0.53	−0.43	1.7	1.5
JJA	0.93	0.96	−0.03	−0.05	0.88	0.88
SON	0.97	0.98	−0.02	−0.06	0.96	1.26
DJF	0.96	0.88	−0.39	−0.53	1.49	1.79
North China (NC)						
ANN	0.97	0.99	−0.14	−0.16	0.68	0.86
MAM	0.95	0.98	−0.44	−0.54	1.55	1.8
JJA	0.91	0.97	−0.06	−0.08	0.97	0.95
SON	0.97	0.99	0.03	0.04	0.79	0.94
DJF	0.98	0.98	−0.11	−0.11	1.18	1.8
Yangtze River Basin (YRB)						
ANN	0.85	0.95	−0.11	−0.06	0.63	0.60
MAM	0.81	0.94	−0.3	−0.29	1.22	1.18
JJA	0.64	0.9	−0.09	0.04	0.91	0.81
SON	0.89	0.94	−0.01	−0.004	0.85	0.85
DJF	0.91	0.94	−0.05	−0.03	1.14	1.6
Southeast China (SE)						
ANN	0.95	0.98	−0.1	−0.001	0.54	0.38
MAM	0.96	0.98	−0.24	−0.17	0.99	0.82
JJA	0.66	0.94	−0.02	0.09	0.6	0.6
SON	0.94	0.97	−0.07	0.04	0.87	0.77
DJF	0.97	0.98	−0.09	0.01	1.2	1.33
Southwest China (SW)						
ANN	0.95	0.99	−0.08	0.003	0.6	0.5
MAM	0.93	0.98	−0.15	−0.08	1.19	1.14
JJA	0.96	0.99	−0.03	0.07	0.6	0.6
SON	0.96	0.99	−0.04	0.04	0.76	0.97
DJF	0.94	0.98	−0.13	−0.04	1.26	1.28
Tibetan Plateau (TP)						
ANN	0.77	0.96	−0.17	−0.04	1.00	0.79
MAM	0.77	0.96	−0.15	−0.07	1.65	1.36
JJA	0.72	0.94	−0.2	−0.04	1.10	1.23
SON	0.77	0.96	−0.14	0.01	1.17	1.29
DJF	0.76	0.88	−0.24	−0.09	1.78	1.57
Northwest China (NW)						
ANN	0.81	0.94	−0.06	−0.06	0.66	0.83
MAM	0.81	0.96	−0.29	−0.36	1.52	1.71
JJA	0.83	0.97	0.04	0.03	0.73	0.83
SON	0.81	0.96	0.1	0.12	0.90	1.03
DJF	0.72	0.72	−0.14	−0.09	1.29	1.83

All the correlation coefficients are statistically significant

**Fig. 4** Same as Fig. 2, but for summer precipitation (units: mm)



observed among the observations, particularly between GPCP and other three products, which is related to its resolution. The observations indicate two peaks of frequency in rainfall amounts of <math><0.5</math> and <math>2.5\text{--}3.5</math> mm/day, separately. MIROC5 and WRF reproduce the main features of precipitation probability distribution; however, they underestimate the frequency of light rainfall (<math><0.5</math> mm/day) and overestimate the frequency of heavy rainfall (>8 mm/day). The bias feature is also observed in the probability distribution of domain-averaged daily precipitation over eastern China (Fig. 7b), which shows positive bias in the frequency of the light rainfall but negative one in the frequency of the heavy rainfall.

The annual mean precipitation trend for 1976–2005 is compared based on observations and model simulations. The reason why we use the period of 1976–2005 instead of 1986–2005 is that a lot of previous research indicated a decadal shift of precipitation over eastern part of China in

the late 1970s, with the precipitations increase in the Yangtze River Valley and decrease in North China (Wang 2001; Ding et al. 2009), which can be found in the observations in Fig. 8. The observation also shows that the annual precipitation increases over Southeast China and the eastern edge of the Tibetan Plateau, while decreases in central China and Southwest China. When focusing on the model simulation, MIROC5 can reproduce some features of precipitation change, but the wet trend over North China is opposite to the observation. WRF simulation exhibits much better agreement with the observation, including more precipitation in the lower reaches of Yellow River Valley, the Yangtze River Valley, Southeast China, and the eastern edge of the Tibetan Plateau and less precipitation in North China and Southwest China. Considering the trend is of fundamental importance in our future projection estimations, this significant improvement indicates more confidence of the robustness for WRF in future projection simulations.

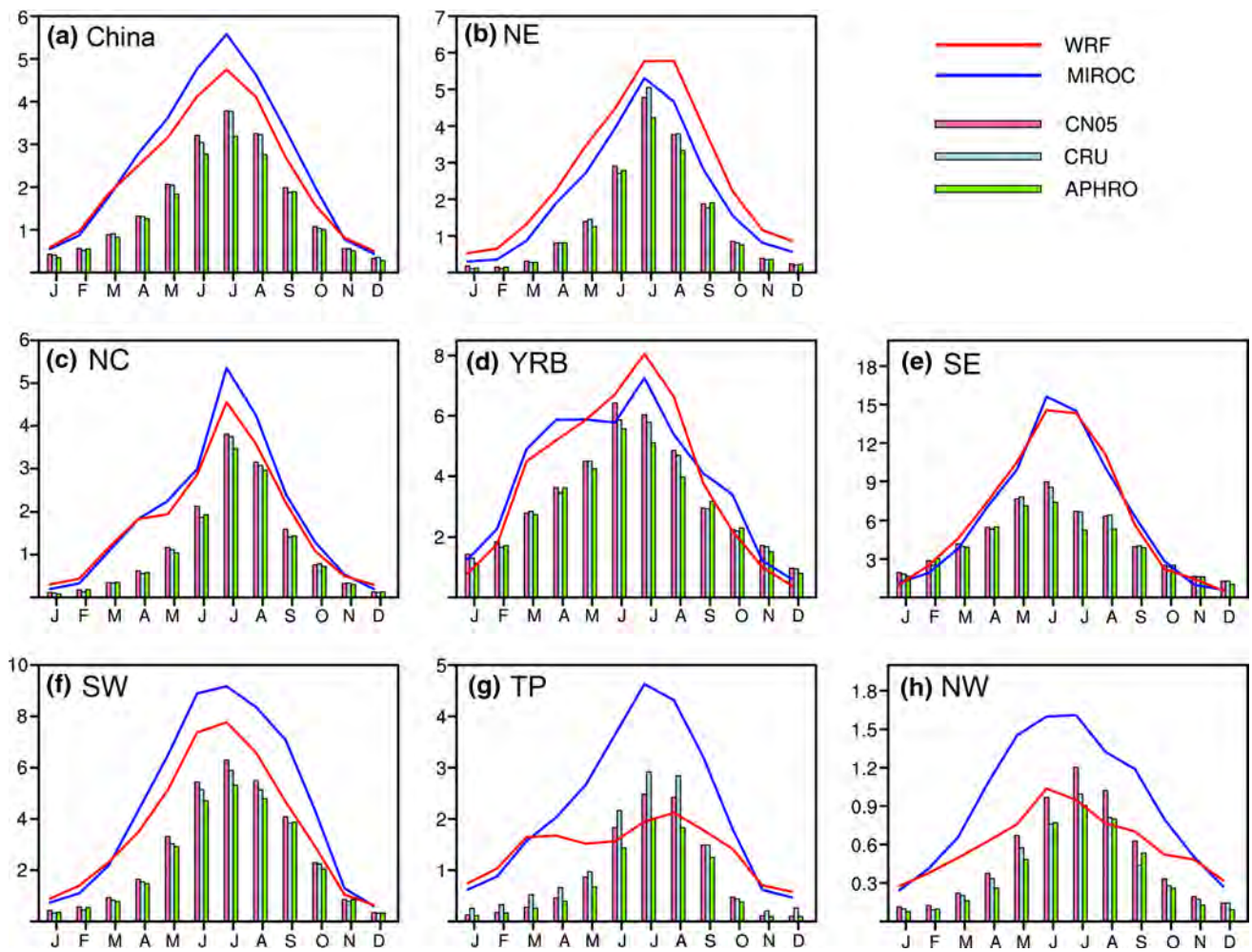


**Fig. 5** The annual cycle of precipitation (units: mm/day) from observation and model simulations for China (a) and the sub-regions (b–h)

### 3.2.2 Bias analysis

WRF can generally reproduce spatial distribution, variation and trend of precipitation over China, however, there are biases between the simulation and observation, with overestimation in Southeast China, while underestimation in the middle latitude of China in summer (Fig. 4f). The biases are revealed by the model simulation of atmospheric circulation and moisture transport in summer.

The pressure–latitude cross-section of the summer mean zonal and meridional wind averaged over 110°–130° from CFSR and WRF is illustrated in Fig. 9. The zonal cross-section is occupied by the westerly winds across the whole troposphere, except for the easterly wind in the low latitude above 500 hPa in the observation. The meridional winds are southerly wind in the low troposphere in the low latitude, and northerly wind in the middle troposphere in the middle latitude. Southerly wind is observed in upper troposphere in high latitude. WRF can generally

reproduce the main features of wind distribution, however, there are differences between the observed data and the simulation.

For the zonal wind, the subtropical westerly jet at 200 hPa in WRF is stronger, with the center moving southward, and the westerly winds in the low troposphere are weaker in low latitude while stronger in the middle latitude (Fig. 9). For the meridional wind, the simulated southerly wind centre in the low troposphere in low latitude is stronger than the observation, and is weaker in the middle latitude.

The simulated strong subtropical westerly jet and strong southerly wind centre in low troposphere are linked with the southerly and easterly wind anomaly in low troposphere in low latitude and northerly and westerly wind anomaly in the middle latitude. This wind biases affected the atmospheric circulation simulation and moisture transport, which is closely connected to the summer precipitation in eastern part of China.

**Fig. 6** Latitude–time cross-section of the precipitation (unit: mm/day) average over the regions of 110°–125°E from the observation (a–d) and the corresponding model–observation differences (e, f)

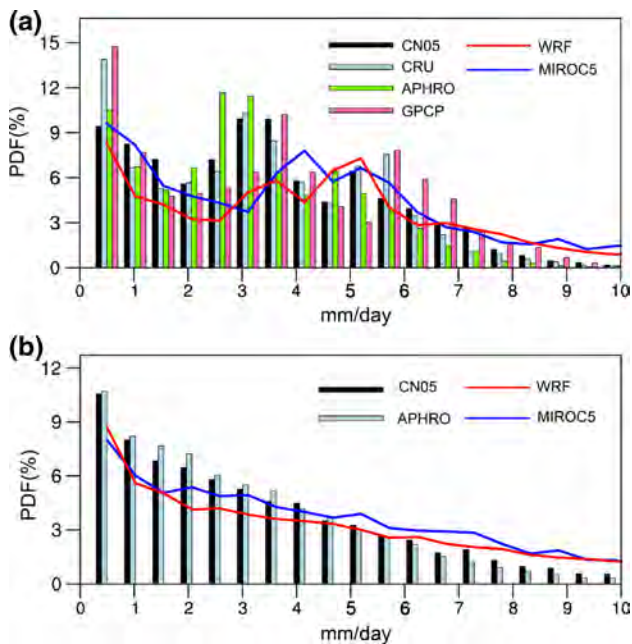
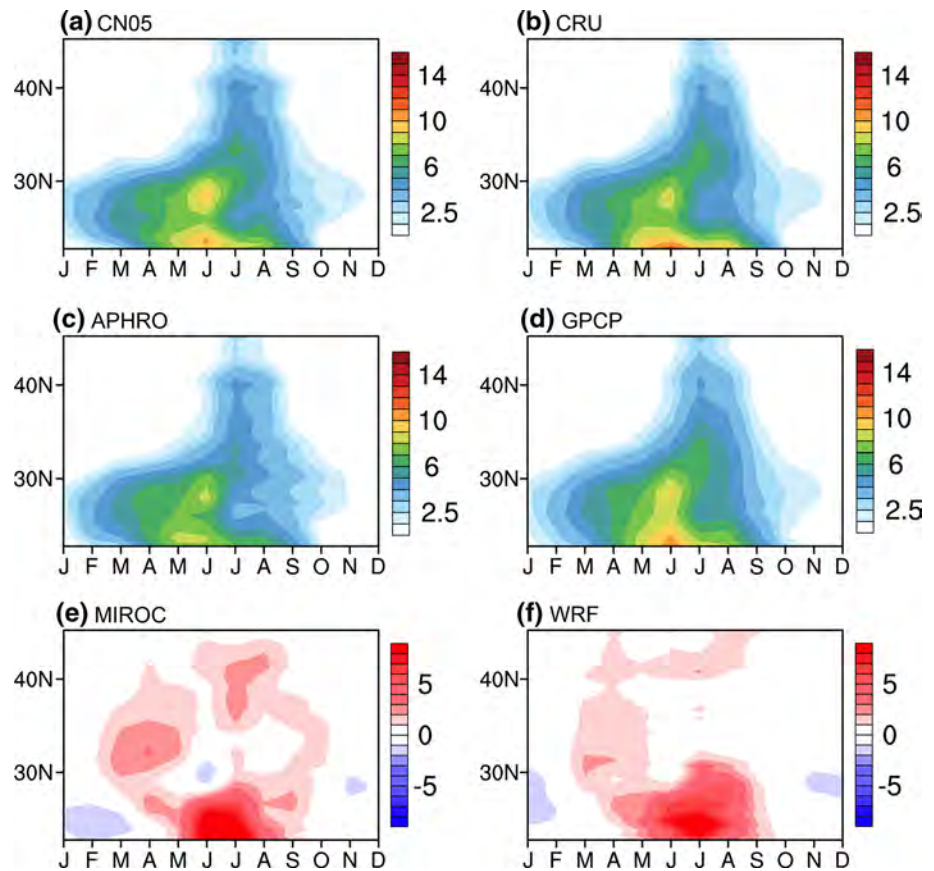
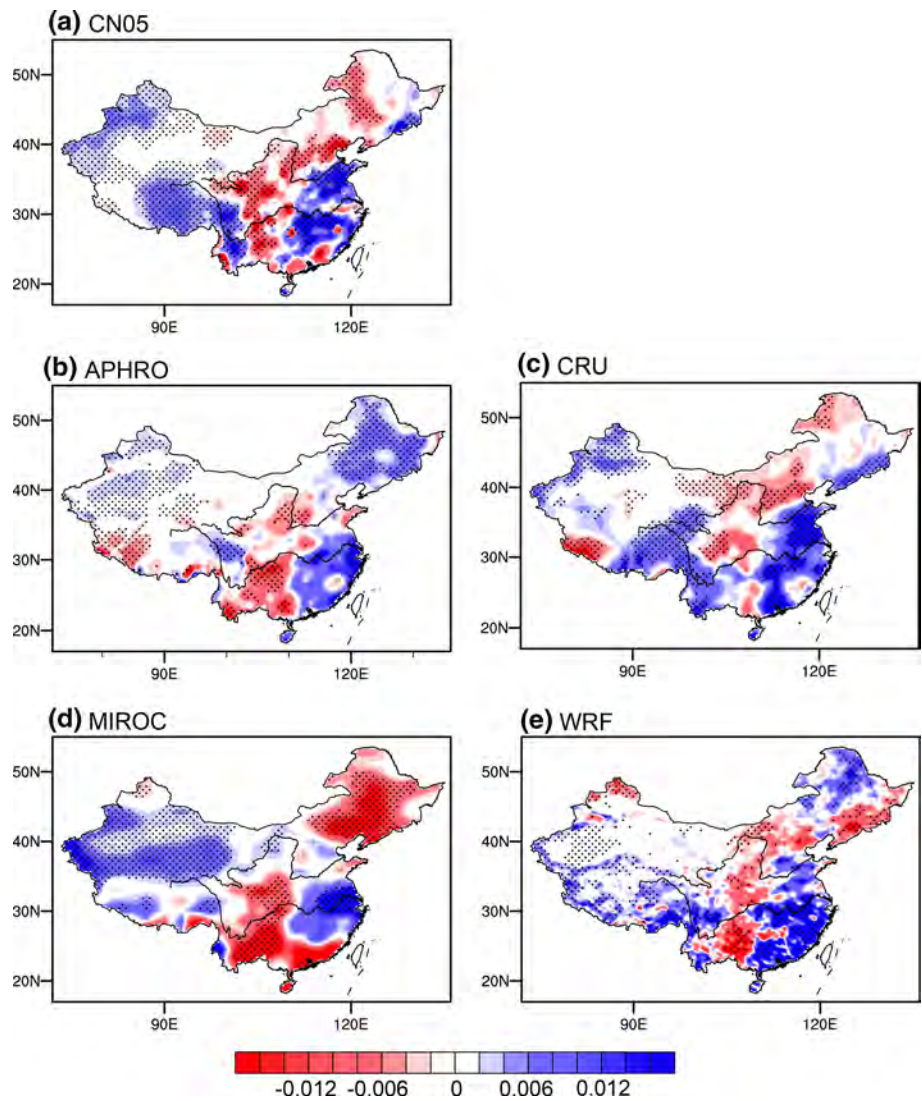


**Fig. 7** **a** Probability distribution of temporal averaged precipitation, **b** probability distribution of domain-averaged daily precipitation over China. CN05 and APHRO are used due to the availability of daily precipitation

The spatial distribution of zonal wind and model bias at 200 hPa indicate WRF overestimates the subtropical westerly jet and the centre is south to the observation (Fig. 10a–c). For the zonal wind at 850 hPa, a negative bias belt exists at the low latitude of China. Compared with CFSR data, westerly wind is stronger and extends far southward, as a result, a positive bias belt exists in the middle latitude. For the meridional wind at 850 hPa, the simulated southerly winds in Southeast China are considerable stronger than the observation. With the negative bias of zonal wind, there is a positive bias of southeasterly flow in southeast China. WRF overestimates the westerly wind in the middle latitude, but underestimates the southerly wind, therefore, a northwesterly wind bias exists in the middle latitude of China.

For the moisture transport at 850 hPa, the strong southeasterly flow results in stronger moisture transport in Southeast China, which exists a strong positive bias and has significant effect on the positive precipitation bias in the region. On the other hand, WRF shows a strong negative bias for moisture transport in the middle latitude of China, exhibiting less moisture transport in this region. What is more, there exists strong negative bias of specific humidity in WRF simulation (Fig. 10m–o), this model bias results in the negative bias of precipitation in the middle latitude of China.

**Fig. 8** Annual precipitation trend for 1976–2005 from **a** CN05, **b** APHRO, **c** CRU, **d** MIROC5 and **e** WRF for JJA. *Dots* indicate the significance level is higher than 90 %



### 3.3 Climate extremes

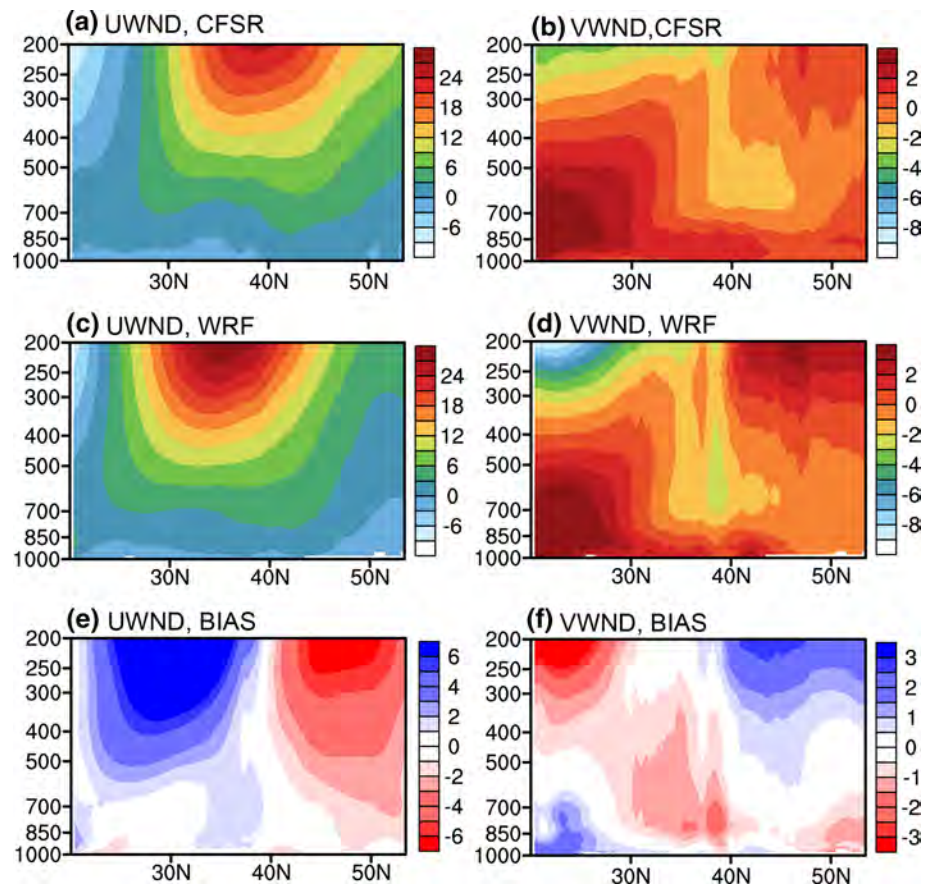
To determine the model’s performances in simulating climate extremes, several climate extremes indices were computed, namely number of tropical nights (TR), cold spell duration index (CSDI), percentage of days when daily minimum temperature lower than 10th percentile of daily minimum temperature (TN10P), percentage of days when daily maximum temperature greater than 90th percentile of daily maximum temperature (TX90P), number of summer days (SU), number of icing days (ID), annual count of days when daily precipitation greater than 10 mm (R10mm), maximum length of wet spell (CWD), annual account of precipitation when daily precipitation greater than 95th percentile of daily precipitation (R95PTOT), monthly maximum consecutive 5-day precipitation (RX5DAY). Further details of these indices have been reported by Karl et al. (1999). Because the indices require maximum temperature,

minimum temperature, and precipitation observations on daily scale, we used CN05 products as the observation.

The spatial distribution of tropical nights (TR) derived from the observation indicates that TR is more in the low latitude, ranging from Southeast China and Southwest China to the Yangtze River Valley (Fig. 11a). For MIROC5 simulation, TR is generally overestimated, the larger positive biases cover Southeast China, the Yangtze River Valley, North China, Northeast China and Northwest China. Improvement of TR simulation is observed in WRF simulation, with the regions where the model has biases covering less area than that of MIROC5, especially in North China, Northeast China and Northwest China (Fig. 11e).

For the simulation of cold spell duration index (CSDI), MIROC5 mainly shows positive bias over China, especially over the Tibetan Plateau, meanwhile, the regions where CSDI is underestimated cover the Northeast China and Northwest China. In WRF simulation, the regions where

**Fig. 9** Pressure–latitude cross-section of the zonal (a, c, e) and meridional winds (b, d, f) average over the regions of 110°–130° in summer for CFSR (a, b), WRF (c, e), and the biases (c, f) model minus observation, unit:  $\text{m s}^{-1}$



CSDI is overestimated cover less area with less biases, especially over the Tibetan Plateau. The correlation coefficient for WRF is 0.80, which indicates better performance of WRF compared with MIROC5 (0.75 in Fig. 11d).

For the percentile type extreme temperature indices, TN10P and TX90P were calculated. TN10P is larger in the regions of Southeast China, Southwest China and central China in the observation. MIROC5 shows mostly positive biases over China, especially in Southwest Tibet. However, in the WRF simulation, the regions where TN10P is overestimated exhibits less biases, resulting in higher correlation coefficient in WRF (0.96) compared with MIROC5 (0.94).

Spatial distribution of TX90P derived from the observation indicates that TX90P is larger in North China and eastern part of Northwest China (Fig. 12). Consistent underestimations are found in MIROC5 simulation over China. However, the regions where TX90P is underestimated cover less area in the WRF simulation, especially over Southeast China, North China, the Tibetan Plateau, and eastern part of Northwest China. The range of biases in WRF simulation is also smaller than that in MIROC5, thus WRF shows better performance with high correlation coefficient (0.99) compared with MIRCO5 (0.98).

Summer days number (SU) from the observation reveals similar distribution with the summer mean temperature

(Fig. 2a). These features are well reproduced by MIROC5 and WRF, however, SU is generally overestimated by MIROC5, with the exception of Southeast China and Northwest China. For WRF simulation, consistent underestimation is observed over China, the maximum negative biases are located in Tarim Basin and Southwest China, which is similar with the MIROC5 simulation, however, the correlation coefficient is much higher in WRF (0.97) compared with MIROC5 (0.90 in Fig. 13e).

For icing days number (ID) simulation, both MIROC5 and WRF generally overestimate ID, especially over the Tibetan Plateau. Meanwhile, WRF shows better similarity with the observation with higher correlation coefficient (Fig. 13f).

R10mm derived from the observation shows similar distribution with the precipitation (Fig. 4a), with more R10mm in Southeast China and less in Northwest China (Fig. 14a). Both MIROC5 and WRF overestimate R10mm, especially over Southwest China and the Tibetan Plateau. The regions where R10mm is overestimated in WRF simulation cover less area with smaller bias range, which results in higher correlation coefficient in WRF simulation (0.91) than that in MIROC5 (0.89 in Fig. 14f).

Observed maximum length of wet spell (CWD) indicates more CWD over Southeast China and the Tibetan

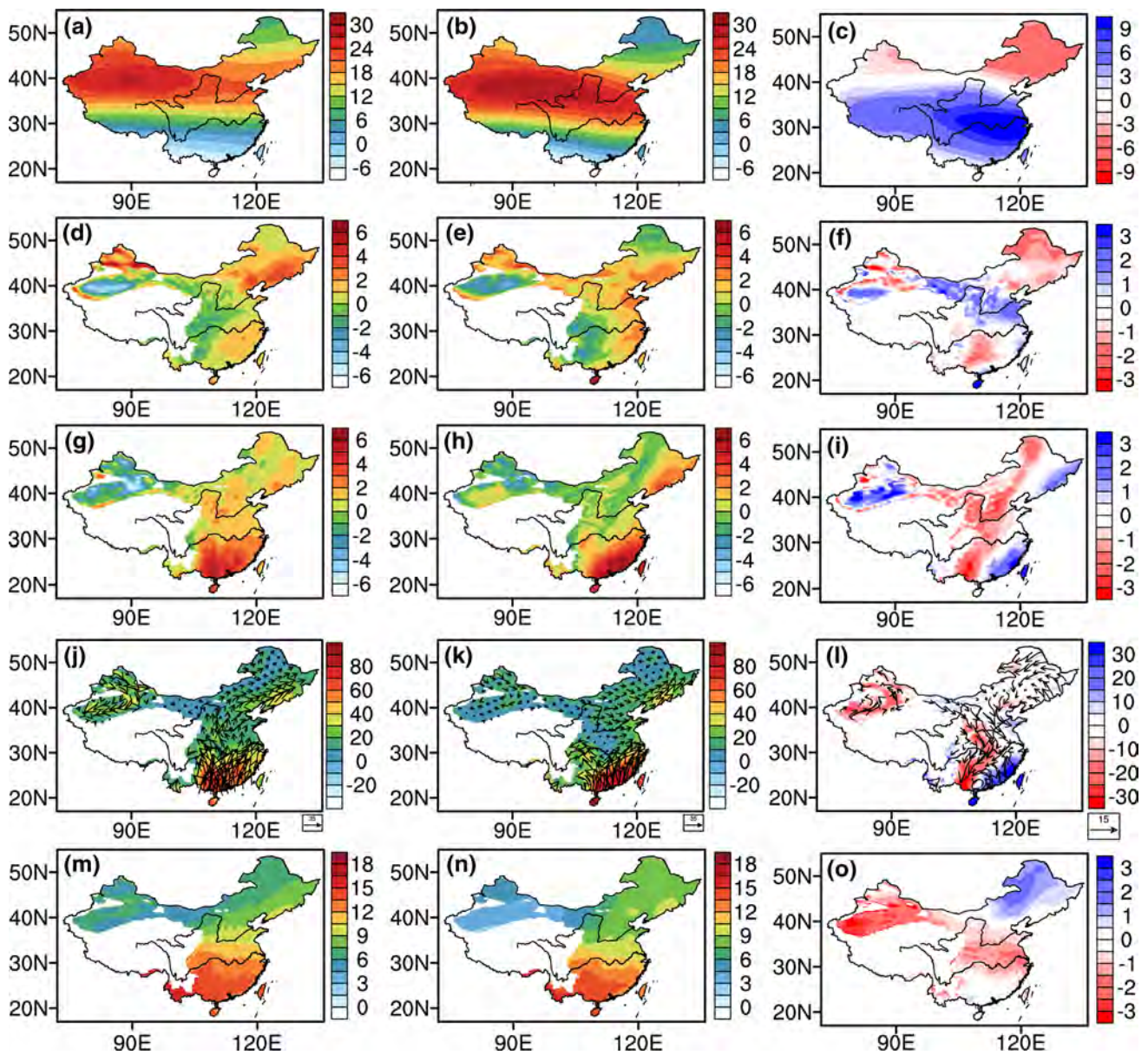


**Fig. 10** Observed (a, d, g, j, m) and simulated (b, e, h, k, n) zonal winds at 200 hPa (a–c, unit:  $\text{m s}^{-1}$ ), zonal winds (d–f, unit:  $\text{m s}^{-1}$ ), meridional winds (g–i, unit:  $\text{m s}^{-1}$ ), the water vapor flux (shaded) and

vector (j–l, unit:  $\text{g m}^{-1} \text{s}^{-1}$ ), and specific humidity (m–o, unit:  $\text{g/kg}$ ) at 850 hPa in summer along with the bias (c, f, i, l, o)

Plateau, and less over Northwest China. This distribution can be reproduced by MIROC5, however, CWD is generally overestimated, except for the regions in Southeast China and Southwest China. There are improvements in WRF simulation over Southeast China, the Yangtze River Valley and North China, however, WRF shows large negative biases in the Tibetan Plateau (Fig. 14f).

For annual account of precipitation when daily precipitation greater than 95th percentile of daily precipitation (R95PTOT), observation indicates R95PTOT decreases from Southeast China to Northwest China, which is similar

with the precipitation distribution (Fig. 4a). Both MIROC5 and WRF reproduce the distribution of R95PTOT well, however, consistent positive biases can be found in the simulations over China. The maximum overestimation is located in Southwest China and the eastern edge of the Tibetan Plateau. In the regions of North China and central China, the areas where R95PTOT is overestimated cover less area in WRF simulation, and the correlation coefficient is higher in WRF (Fig. 15e). RX5Day derived from the observation indicates that RX5DAY is high in Southeast China and low in Northwest China (Fig. 15b). Both

**Fig. 11** Spatial distribution of TR (**a, c, e**, units: day) and CSDI (**b, d, f**, units: day) climatology (**a, b**) and model-observation differences (model minus observation, **c–f**) during 1986–2005 from the CN05, MIROC5 and WRF, the correlation coefficients between model results and CN05 products are labeled on the *top right*, *asterisk* indicated the significant level is higher than 90 %

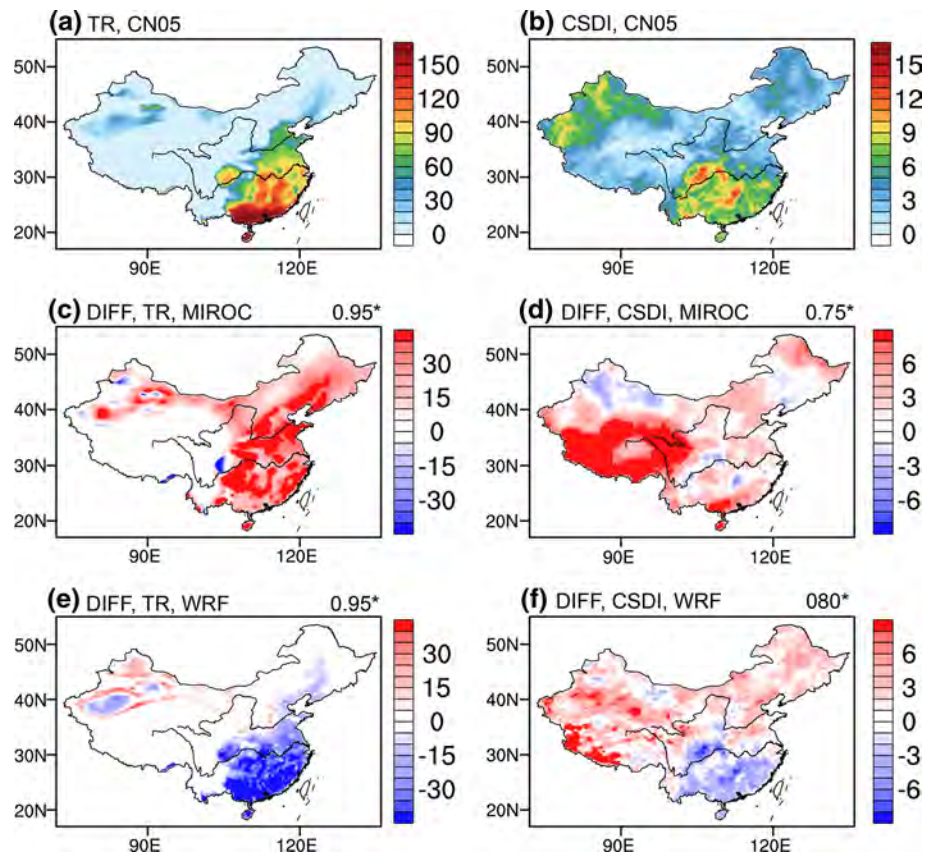


**Fig. 12** Same as Fig. 11, but for TN10P (**a, c, e**, units: %) and TX90P (**b, d, f**, units: %)

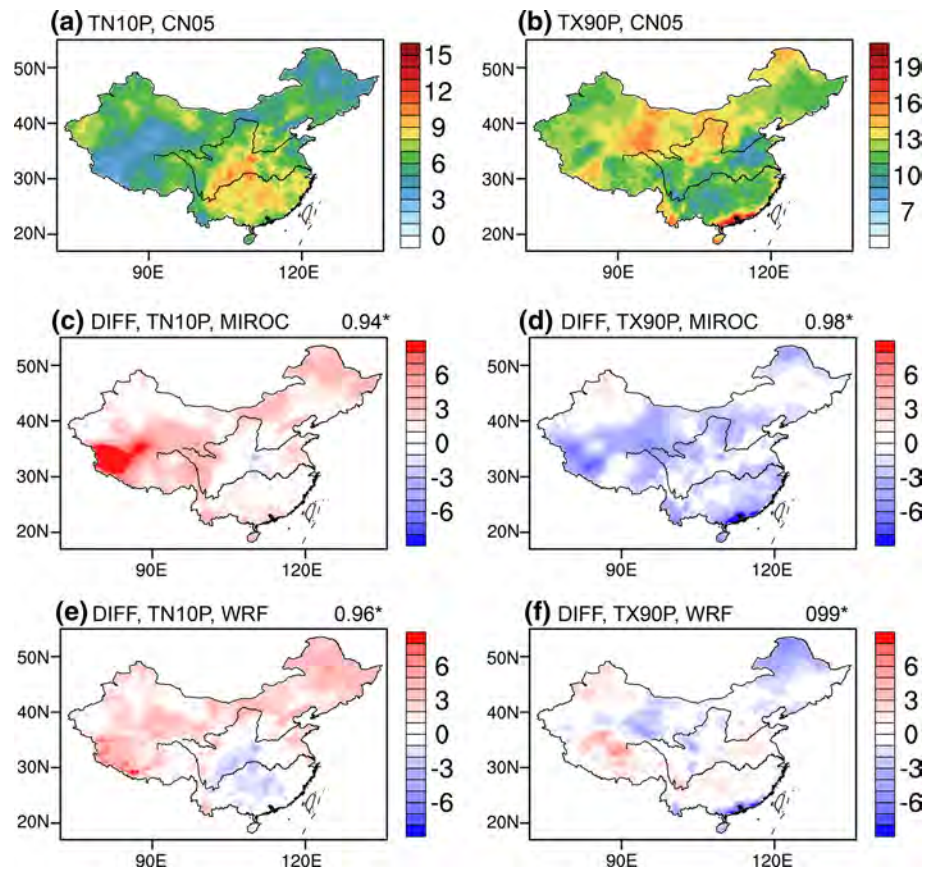


**Fig. 13** Same as Fig. 11, but for SU (a, c, e, units: day) and ID (b, d, f, units: day)

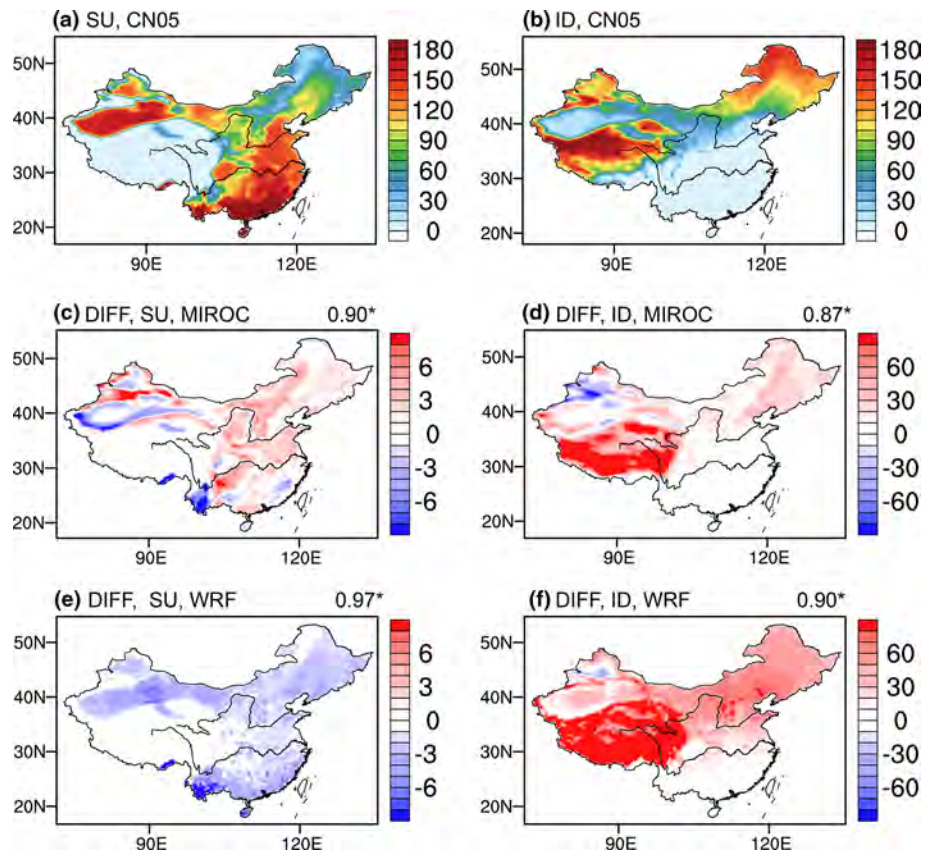


**Fig. 14** Same as Fig. 11, but for R10mm (a, c, e, units: day) and CWD (b, d, f, units: day)

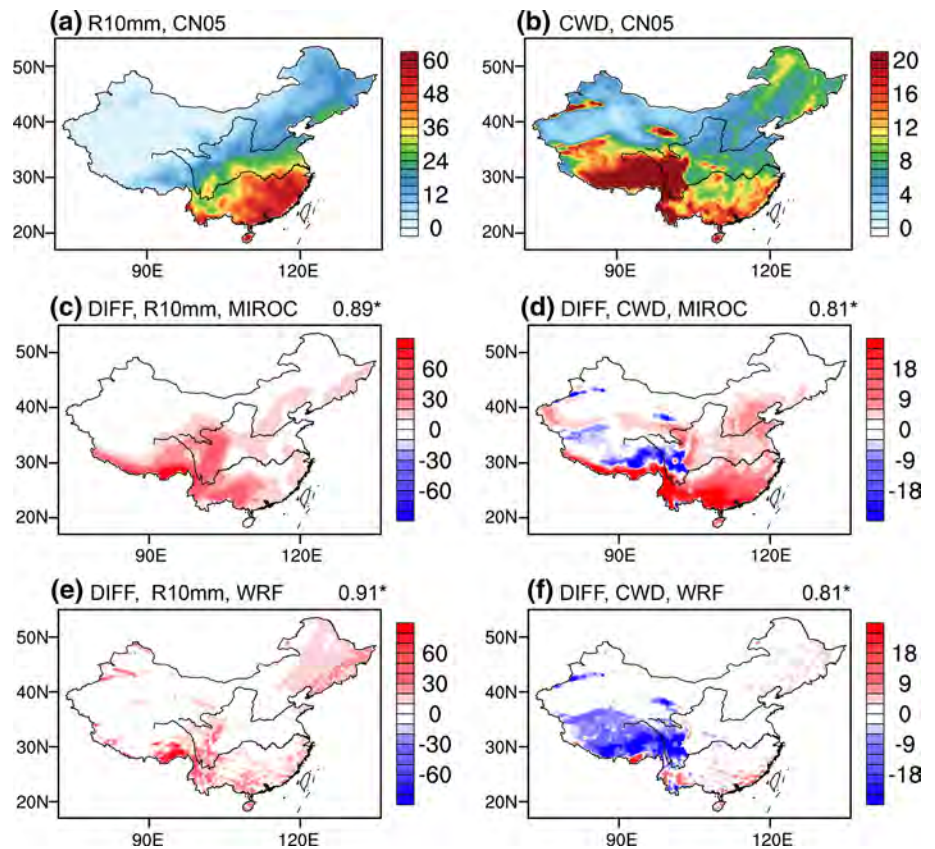
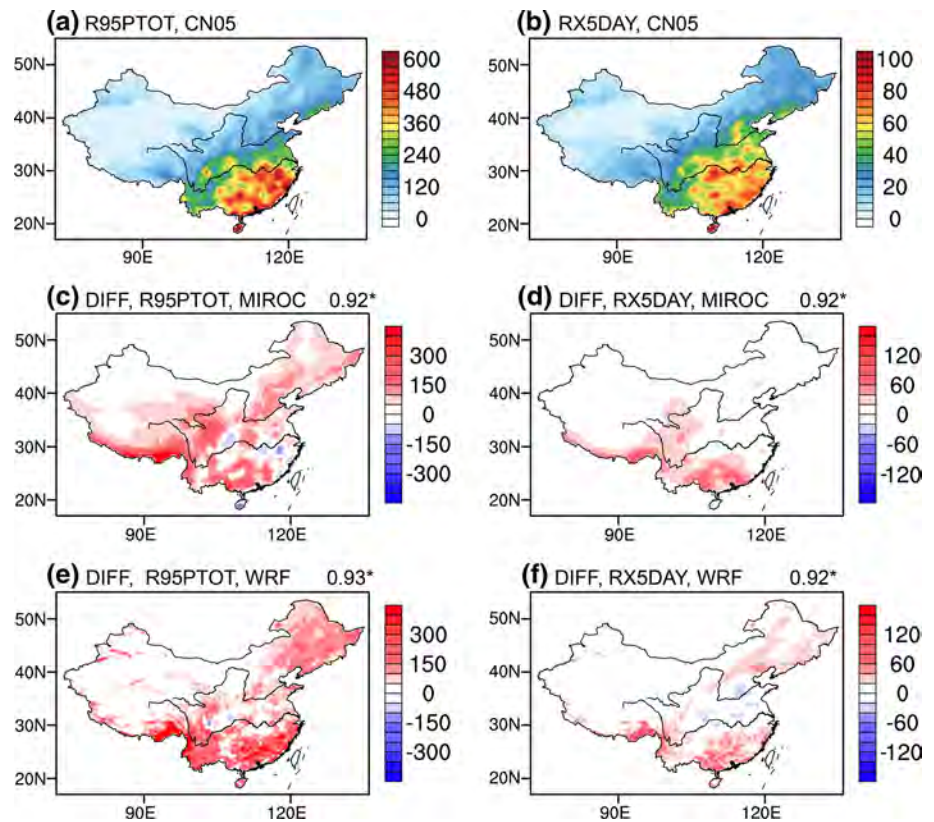


**Fig. 15** Same as Fig. 11, but for R95PTOT (a, c, e, units: mm) and RX5DAY (b, d, f, units: day)



MIROC5 and WRF well reproduce the spatial distribution, with the correlation coefficient of 0.92. However, RX5DAY is generally overestimated by MIROC5 and WRF, the regions where RX5DAY is overestimated cover less area in WRF simulation over Southwest China, and the bias range is smaller in WRF simulation.

#### 4 Conclusion and discussions

Global warming has profound impact on the vulnerable environment in China, robust climate projection is quite important. However, the coarse resolution of the GCMs limits the models' performance in resolving the regional scale atmospheric circulation. High-resolution simulations can improve the model performance (Liu et al. 2012b; Yu 2012; Gao et al. 2011). Meanwhile, future human adaptation assessments require climate change information at the resolution much finer than GCMs can provide.

We completed a long continuous simulation for historical run (1946–2005) and RCP60 run (2006–2100) using WRF, in which the main objectives are to provide multi-model high-resolution future projection simulations and to offer an assessment of climate change over China for adaptation and migration studies. In this paper, the model's ability in simulating the present (1986–2005) climate is validated using historical run and multiple observational products.

We find that MIROC5 can effectively reproduce the spatial distribution of temperature, whereas WRF exhibits much better agreement with the observation, particularly for the regional features in Southeast China and Northwest China. The uncertainties in temperature variability are larger than those in climatology among both the observation products and the simulations. WRF achieves better performances over China and shows better agreement with the observation.

Precipitation decreases from southeast to northwest, and is more in summer and less in winter. The rainfall belt advances and retreats over eastern China due to the monsoon system. For the frequency distribution, the observations indicate two peaks of frequency in rainfall amount of <0.5 and 2.5–3.5 mm/day, separately. MIROC5 reproduce these precipitation features with model deficiency, whereas WRF simulation shows better performance, particularly at the regional scale. WRF shows obvious wet bias in precipitation in Southeast China and the middle latitude of eastern China, which can be explained by biases in atmospheric circulation and water vapor transport. The spatial distributions of several extreme climate indices are effectively reproduced by MIROC5 and WRF. In addition, improvements are observed in the later simulation, this significant improvement gives us more confidence in RCM simulation for future projection.

It is important that in the continuous simulation, the boundary conditions of the MIROC5 outputs were used

other than reanalysis data; therefore, the boundary conditions could not be considered as “perfect” conditions. Previous studies revealed that the bias of GCM can be transferred to RCM (Liu et al. 2012b; Berg et al. 2013; Liang et al. 2008), the better performance of RCM emphasizes the importance of the finer-scale surface forcing in producing realistic small-scale features (Argueso et al. 2012; Kim et al. 2013; Gao et al. 2008). This validation also indicates the potential value of high-resolution simulation for application in future adaptation and migration studies.

In addition, there are large uncertainties in the simulation over the Tibetan Plateau and Northwest China. Apart from the model deficiency over these regions, we should also consider the uncertainties in the observations because the stations are sparse and are always located in the lowland over these regions (Yu 2012; Wu et al. 2011). This uncertainty jeopardizes our ability to extensively investigate the regional climate over these regions and demonstrates the importance of accurate measurements and proper setup of the observation stations.

Finally, because uncertainties remain in the precipitation simulations discussed above and in previous studies (Gao et al. 2011; Liu et al. 2012b), future projection should be interpreted with caution. According to our evaluation, the agreement is better in temperature simulation than that in precipitation, and the model performance is better in simulating the climatology than that for variability and trends. Considering the uncertainties in the RCM itself and those transferred from the GCM, regional model ensembles at high resolution should be conducted in future studies to reduce the uncertainties and to provide more robust climate projections.

**Acknowledgments** This work was supported by the National Basic Research Program of China (2012CB955401), the Special Fund for Public Welfare Industry (GYHY201306026), the National Natural Science Foundation of China (41320104007), ‘the Jiangsu Collaborative Innovation Center for Climate Chang’ and KLOE Open Fund (XJDX0201-2012-04). We thank Dr. Manabu Abe of Japan’s National Institute for Environmental Studies for providing the MIROC5 data, we are also thankful to the anonymous reviewers for their helpful comments on the former version of this manuscript.

## References

- Argueso D, Hidalgo-Munoz JM, Gamiz-Fortis SR, Esteban-Parra MJ, Castro-Diez Y (2012) High-resolution projections of mean and extreme precipitation over Spain using the WRF model (2070–2099 versus 1970–1999). *J Geophys Res*. doi:10.1029/2011jd017399
- Berg P, Wagner S, Kunstmann H, Schadler G (2013) High resolution regional climate model simulations for Germany: part I—validation. *Clim Dyn* 40(1–2):401–414. doi:10.1007/s00382-012-1508-8
- Caldwell P, Chin H, Bader D, Bala G (2009) Evaluation of a WRF dynamical downscaling simulation over California. *Clim Change* 95(3–4):499–521. doi:10.1007/s10584-009-9583-5
- Chen H (2013) Projected change in extreme rainfall events in China by the end of the 21st century using CMIP5 models. *Chin Sci Bull* 58:1–10. doi:10.1007/s11434-012-5612-2
- Chen Q, Li Z, Fan G, Zhu K, Zhang W, Zhu H (2011) Indications of stratospheric anomalies in the freezing rain and snow disaster in South China, 2008. *Sci China Earth Sci* 54(8):1248–1256. doi:10.1007/s11430-011-4192-3
- Chen H, Sun J, Chen X (2013) Future changes of drought and flood events in China under a global warming scenario. *Atmos Oceanic Sci Lett* 6(1):8–13
- Collins W, Rasch P, Boville B, Hack J, McCaa J, Williamson D, Kiehl J, Briegleb B, Bitz C, Lin S (2004) Description of the NCAR community atmosphere model (CAM 3.0). NCAR Tech Note NCAR/TN-464+STR
- Ding Y, Chan JCL (2005) The East Asian summer monsoon: an overview. *Meteorol Atmos Phys* 89(1–4):117–142. doi:10.1007/s00703-005-0125-z
- Ding Y, Wang Z, Song Y, Zhang J (2008) Causes of the unprecedented freezing disaster in January 2008 and its possible association with the global warming. *Acta Meteorol Sinica* 66(5):808–825
- Ding Y, Sun Y, Wang Z, Zhu Y, Y Song (2009) Inter-decadal variation of the summer precipitation in China and its association with decreasing Asian summer monsoon. Part II: possible causes. *Int J Climatol*. doi:10.1002/joc.1759
- Endris HS, Omondi P, Jain S, Lennard C, Hewitson B, Chang’a L, Awange JL, Dosio A, Ketiemi P, Nikulin G, Panitz H-J, Büchner M, Stordal F, Tazalika L (2013) Assessment of the performance of CORDEX regional climate models in simulating East African rainfall. *J Clim* 26(21):8453–8475. doi:10.1175/JCLI-D-12-00708.1
- Fu Y, Lu R, Wang H, Yang X (2013) Impact of overestimated ENSO variability in the relationship between ENSO and East Asian summer rainfall. *J Geophys Res* 118(12):6200–6211. doi:10.1002/jgrd.50482
- Gao X, Shi Y, Song R, Giorgi F, Wang Y, Zhang D (2008) Reduction of future monsoon precipitation over China: comparison between a high resolution RCM simulation and the driving GCM. *Meteorol Atmos Phys* 100(1–4):73–86. doi:10.1007/s00703-008-0296-5
- Gao X, Shi Y, Giorgi F (2011) A high resolution simulation of climate change over China. *Sci China Earth Sci* 54(3):462–472. doi:10.1007/s11430-010-4035-7
- Gao Y, Fu J, Drake J, Liu Y, Lamarque J (2012a) Projected changes of extreme weather events in the eastern United States based on a high resolution climate modeling system. *Environ Res Lett* 7(4):044025
- Gao X, Shi Y, Zhang D, Giorgi F (2012b) Climate change in China in the 21st century as simulated by a high resolution regional climate model. *Chin Sci Bull* 57(10):1188–1195. doi:10.1007/s11434-011-4935-8
- Ge Q, Zhang X, Zheng J (2013) Simulated effects of vegetation increase/decrease on temperature changes from 1982 to 2000 across the Eastern China. *Int J Climatol* 34(1):187–196. doi:10.1002/joc.3677
- Giorgi F, Jones C, Asrar GR (2009) Addressing climate information needs at the regional level: the CORDEX framework. *WMO Bull* 58:175–183
- He S, Wang H (2013) Oscillating relationship between the East Asian winter monsoon and ENSO. *J Clim* 26(24):9819–9838. doi:10.1175/JCLI-D-13-00174.1
- Hong S-Y, Lim J-OJ (2006) The WRF Single-Moment 6-Class Microphysics Scheme (WSM6). *J Korean Meteor Soc* 42:129–151
- Hong SY, Noh Y, Dudhia J (2006) A new vertical diffusion package with an explicit treatment of entrainment processes. *Mon Wea Rev* 134(9):2318–2341. doi:10.1175/MWR3199.1
- Hu A, Li N, Zhu Y, Wu J, Guo H, Li C (2010) Integrated risk governance paradigm for meteorological disasters: thoughts on the

- low-temperature freezing rain and snow disaster in Southern China of 2008. *Prog Geogr* (in Chinese) 29(2):159–165
- Huffman GJ, Bolvin DT, Nelkin EJ, Wolff DB, Adler RF, Gu G, Hong Y, Bowman KP, Stocker EF (2007) The TRMM multisatellite precipitation analysis (TMPA): quasi-global, multiyear, combined-sensor precipitation estimates at fine scales. *J Hydrometeorol* 8(1):38–55. doi:[10.1175/JHM560.1](https://doi.org/10.1175/JHM560.1)
- Huffman GJ, Adler RF, Bolvin DT, Gu G (2009) Improving the global precipitation record: GPCP Version 2.1. *Geophys Res Lett* 36(17):L17808. doi:[10.1029/2009GL040000](https://doi.org/10.1029/2009GL040000)
- IPCC (2013) Climate Change 2013: The physical science basis. In: Stocker TF, Qin D, Plattner G-K, Tignor M, Allen SK, Boschung J, Nauels A, Xia Y, Bex V, Midgley PM (eds) Contribution of working group I to the fifth assessment report of the intergovernmental panel on climate change. Cambridge University Press, Cambridge
- Joyce RJ, Janowiak JE, Arkin PA, Xie P (2004) CMORPH: a method that produces global precipitation estimates from passive microwave and infrared data at high spatial and temporal resolution. *J Hydrometeorol* 5(3):487–503
- Kain JS (2004) The Kain-Fritsch convective parameterization: an update. *J Appl Meteorol* 43(1):170–181
- Karl T, Nicholls N, Ghazi A (1999) CLIVAR/GCOS/WMO workshop on indices and indicators for climate extremes workshop summary. In: Karl T, Nicholls N, Ghazi A (eds) weather and climate extremes. Springer, Dordrecht, pp 3–7. doi:[10.1007/978-94-015-9265-9\\_2](https://doi.org/10.1007/978-94-015-9265-9_2)
- Kim J, Waliser D, Mattmann C, Goodale C, Hart A, Zimdars P, Crichton D, Jones C, Nikulin G, Hewitson B, Jack C, Lennard C, Favre A (2013) Evaluation of the CORDEX-Africa multi-RCM hindcast: systematic model errors. *Clim Dyn*. doi:[10.1007/s00382-013-1751-7](https://doi.org/10.1007/s00382-013-1751-7)
- Lee J-W, Hong S-Y, Chang E-C, Suh M-S, Kang H-S (2014) Assessment of future climate change over East Asia due to the RCP scenarios downscaled by GRIMs-RMP. *Clim Dyn* 42(3–4):733–747. doi:[10.1007/s00382-013-1841-6](https://doi.org/10.1007/s00382-013-1841-6)
- Liang X, Kunkel KE, Meehl GA, Jones RG, Wang JXL (2008) Regional climate models downscaling analysis of general circulation models present climate biases propagation into future change projections. *Geophys Res Lett* 35(8):L08709. doi:[10.1029/2007GL032849](https://doi.org/10.1029/2007GL032849)
- Liu J, Curry JA, Wang H, Song M, Horton RM (2012a) Impact of declining Arctic sea ice on winter snowfall. *Proc Natl Acad Sci* 109(11):4074–4079. doi:[10.1073/pnas.1114910109](https://doi.org/10.1073/pnas.1114910109)
- Liu S, Gao W, Liang X-Z (2012b) A regional climate model downscaling projection of China future climate change. *Clim Dyn*. doi:[10.1007/s00382-012-1632-5](https://doi.org/10.1007/s00382-012-1632-5)
- Martynov A, Laprise R, Sushama L, Winger K, Šeparović L, Dugas B (2013) Reanalysis-driven climate simulation over CORDEX North America domain using the Canadian Regional Climate Model, version 5: model performance evaluation. *Clim Dyn* 41(11–12):2973–3005. doi:[10.1007/s00382-013-1778-9](https://doi.org/10.1007/s00382-013-1778-9)
- Mitchell TD, Jones PD (2005) An improved method of constructing a database of monthly climate observations and associated high-resolution grids. *Int J Climatol* 25(6):693–712. doi:[10.1002/joc.1181](https://doi.org/10.1002/joc.1181)
- Niu G, Yang Z, Mitchell KE, Chen F, Ek MB, Barlage M, Kumar A, Manning K, Niyogi D, Rosero E, Tewari M, Xia Y (2011) The community Noah land surface model with multiparameterization options (Noah-MP): 1. Model description and evaluation with local-scale measurements. *J Geophys Res* 116(D12):D12109. doi:[10.1029/2010JD015139](https://doi.org/10.1029/2010JD015139)
- Pan L, Chen S, Cayan D, Lin M, Hart Q, Zhang M, Liu Y, Wang J (2011) Influences of climate change on California and Nevada regions revealed by a high-resolution dynamical downscaling study. *Clim Dyn* 37(9–10):2005–2020. doi:[10.1007/s00382-010-0961-5](https://doi.org/10.1007/s00382-010-0961-5)
- Piao S, Ciais P, Huang Y, Shen Z, Peng S, Li J, Zhou L, Liu H, Ma Y, Ding Y, Friedlingstein P, Liu C, Tan K, Yu Y, Zhang T, Fang J (2010) The impacts of climate change on water resources and agriculture in China. *Nature* 467(7311):43–51
- Saha S, Moorthi S, Pan H-L, Wu X, Wang J, Nadiga S, Tripp P, Kistler R, Woollen J, Behringer D, Liu H, Stokes D, Grumbine R, Gayno G, Wang J, Hou Y-T, Chuang H-Y, Juang H-MH, Sela J, Iredell M, Treadon R, Kleist D, Van Delst P, Keyser D, Derber J, Ek M, Meng J, Wei H, Yang R, Lord S, Van Den Dool H, Kumar A, Wang W, Long C, Chelliah M, Xue Y, Huang B, Schemm J-K, Ebisuzaki W, Lin R, Xie P, Chen M, Zhou S, Higgins W, Zou C-Z, Liu Q, Chen Y, Han Y, Cucurull L, Reynolds RW, Rutledge G, Goldberg M (2010) The NCEP Climate Forecast System Reanalysis. *Bull Am Meteorol Soc* 91(8):1015–1057. doi:[10.1175/10BAMS3001.1](https://doi.org/10.1175/10BAMS3001.1)
- Skamarock WC, Klemp JB, Dudhia J, Gill DO, Barker DM, Duda MG, Huang X-Y, Wang W, Powers JG (2008) A description of the advanced research WRF version 3, NCAR technical note
- Sun J (2014) Record-breaking SST over mid-North Atlantic and extreme high temperature over the Jianghuai–Jiangnan region of China in 2013. *Chin Sci Bull*. doi:[10.1007/s11434-014-0425-0](https://doi.org/10.1007/s11434-014-0425-0)
- Sun J, Ao J (2013) Changes in precipitation and extreme precipitation in a warming environment in China. *Chin Sci Bull* 58(12):1395–1401. doi:[10.1007/s11434-012-5542-z](https://doi.org/10.1007/s11434-012-5542-z)
- Sun J, Wang H (2012) Changes of the connection between the summer North Atlantic Oscillation and the East Asian summer rainfall. *J Geophys Res*. doi:[10.1029/2012JD017482](https://doi.org/10.1029/2012JD017482)
- Sun J, Wang H, Yuan W, Chen H (2010) Spatial-temporal features of intense snowfall events in China and their possible change. *J Geophys Res* 115:D16110. doi:[10.1029/2009JD013541](https://doi.org/10.1029/2009JD013541)
- Sun J, Wang H, Yuan W (2011) Decadal variability of the extreme hot event in China and its associated with atmospheric circulation. *Clim Environ Res* (in Chinese) 16:199–208
- Taylor KE, Stouffer RJ, Meehl GA (2011) An overview of CMIP5 and the experiment design. *Bull Am Meteorol Soc* 93(4):485–498. doi:[10.1175/BAMS-D-11-00094.1](https://doi.org/10.1175/BAMS-D-11-00094.1)
- Vautard R, Gobiet A, Jacob D, Belda M, Colette A, Déqué M, Fernández J, García-Díez M, Goergen K, Güttler I, Halenka T, Karacostas T, Katragkou E, Keuler K, Kotlarski S, Mayer S, van Meijgaard E, Nikulin G, Patarčić M, Scinocca J, Sobolowski S, Suklitsch M, Teichmann C, Warrach-Sagi K, Wulfmeyer V, Yiou P (2013) The simulation of European heat waves from an ensemble of regional climate models within the EURO-CORDEX project. *Clim Dyn* 41(9–10):2555–2575. doi:[10.1007/s00382-013-1714-z](https://doi.org/10.1007/s00382-013-1714-z)
- Vörösmarty CJ, Green P, Salisbury J, Lammers RB (2000) Global water resources: vulnerability from climate change and population growth. *Science* 289(5477):284–288. doi:[10.1126/science.289.5477.284](https://doi.org/10.1126/science.289.5477.284)
- Wang H (2001) The weakening of the Asian monsoon circulation after the end of 1970s. *Adv Atmos Sci* 18:376–386
- Wang H, He S (2013) The increase of snowfall in Northeast China after the mid 1980s. *Chin Sci Bull*. doi:[10.1007/s11434-012-5508-1](https://doi.org/10.1007/s11434-012-5508-1)
- Wang H, Yu E, Yang S (2011) An exceptionally heavy snowfall in Northeast China: large-scale circulation anomalies and hindcast of the NCAR WRF model. *Meteorol Atmos Phys* 113(1–2):11–25. doi:[10.1007/s00703-011-0147-7](https://doi.org/10.1007/s00703-011-0147-7)
- Wang T, Wang HJ, Otterå OH, Gao YQ, Suo LL, Furevik T, Yu L (2013) Anthropogenic agent implicated as a prime driver of shift in precipitation in eastern China in the late 1970s. *Atmos Chem Phys* 13(24):12433–12450. doi:[10.5194/acp-13-12433-2013](https://doi.org/10.5194/acp-13-12433-2013)
- Watanabe M, Suzuki T, Oishi R, Komuro Y, Watanabe S, Emori S, Takemura T, Chikira M, Ogura T, Sekiguchi M, Takata K, Yamazaki D, Yokohata T, Nozawa T, Hasumi H, Tatebe H, Kimoto M (2010) Improved climate simulation by MIROC5:

- mean States, variability, and climate sensitivity. *J Clim* 23(23):6312–6335. doi:[10.1175/2010JCLI3679.1](https://doi.org/10.1175/2010JCLI3679.1)
- Wu J, Gao X (2013) A gridded daily observation dataset over China region and comparison with the other datasets. *Chin J Geophys* (in Chinese) 56(4):1102–1111
- Wu J, Gao X, Giorgi F (2011) Climate change over Xinjiang region in the 21st century simulated by a high resolution regional climate model (in Chinese). *J Glaciol Geocryol* 33:479–487
- Xu J, Powell A Jr (2012) Uncertainty estimation of the global temperature trends for multiple radiosondes, reanalyses, and CMIP3/IPCC climate model simulations. *Theor Appl Climatol* 108(3–4):505–518. doi:[10.1007/s00704-011-0548-z](https://doi.org/10.1007/s00704-011-0548-z)
- Xu C, Xu Y (2012) The projection of temperature and precipitation over China under RCP scenarios using a CMIP5 multimodel ensemble. *Atmos Oceanic Sci Lett* 5(6):527–533
- Yang Z, Niu G, Mitchell KE, Chen F, Ek MB, Barlage M, Longuevergne L, Manning K, Niyogi D, Tewari M, Xia Y (2011) The community Noah land surface model with multiparameterization options (Noah-MP): 2. Evaluation over global river basins. *J Geophys Res* 116(D12):D12110. doi:[10.1029/2010JD015140](https://doi.org/10.1029/2010JD015140)
- Yang J, Gong D, Wang W, Hu M, Mao R (2012) Extreme drought event of 2009/2010 over southwestern China. *Meteorol Atmos Phys* 115(3–4):173–184. doi:[10.1007/s00703-011-0172-6](https://doi.org/10.1007/s00703-011-0172-6)
- Yang B, Zhang Y, Qian Y, Huang A, Yan H (2014) Calibration of a convective parameterization scheme in the WRF model and its impact on the simulation of East Asian summer monsoon precipitation. *Clim Dyn*. doi:[10.1007/s00382-014-2118-4](https://doi.org/10.1007/s00382-014-2118-4)
- Yatagai A, Kamiguchi K, Arakawa O, Hamada A, Yasutomi N, Kitoh A (2012) APHRODITE: constructing a long-term daily gridded precipitation dataset for Asia based on a dense network of rain gauges. *Bull Amer Meteorol Soc* 93(9):1401–1415. doi:[10.1175/BAMS-D-11-00122.1](https://doi.org/10.1175/BAMS-D-11-00122.1)
- Yu E (2012) High-resolution seasonal snowfall simulation over Northeast China. *Chin Sci Bull* 58:1–8. doi:[10.1007/s11434-012-5561-9](https://doi.org/10.1007/s11434-012-5561-9)
- Yu E, Wang H, Sun J (2010) A quick report on a dynamical downscaling simulation over China using the nested model. *Atmos Oceanic Sci Lett* 3(6):325–329
- Zhou T, Gong D, Li J, Li B (2009) Detecting and understanding the multi-decadal variability of the East Asian Summer Monsoon: recent progress and state of affairs. *Meteorol Z* 18(4):455–467. doi:[10.1127/0941-2948/2009/0396](https://doi.org/10.1127/0941-2948/2009/0396)
- Zhu Y, Wang H, Zhou W, Ma J (2011) Recent changes in the summer precipitation pattern in East China and the background circulation. *Clim Dyn* 36(7–8):1463–1473. doi:[10.1007/s00382-010-0852-9](https://doi.org/10.1007/s00382-010-0852-9)